Peak effect in 2H-NbSe$_2$

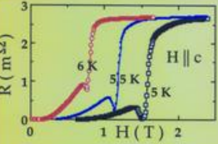

Fixed T; varying H

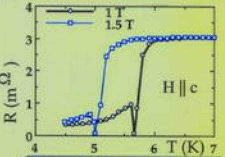

Fixed H; varying T

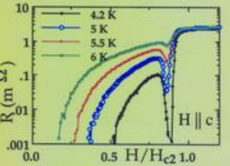

Peak effect in reduced H

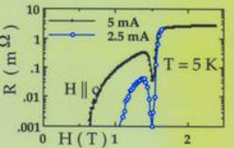

I-dependence of peak effect

* Robust location of resistance minimum in (H,T) space

* Nonlinear; i.e., related to anomalous (H,T)-dependence of pinning

Motion of flux lines : B

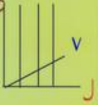

Lorentz Force : $F_L = J \times B$

Overdamped motion : $v \sim \gamma . F$

Electric field : $E = v \times B$, $\parallel J$

Dissipation= Resistance

Intrinsic resistance $R_{ff} = R_n.(H/Hc2)$

Effect of pinning : $V = R_{ff}(I-I_c)$

Expt : Rounded onset

Peak Effect : Different Depinning Process

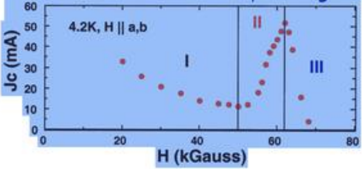

Variation in I-V's

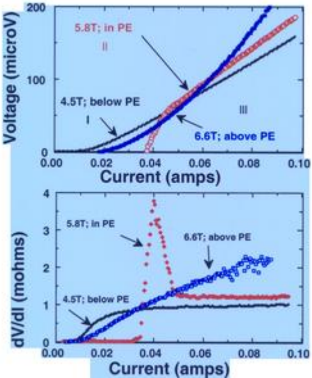

Cha & Fertig

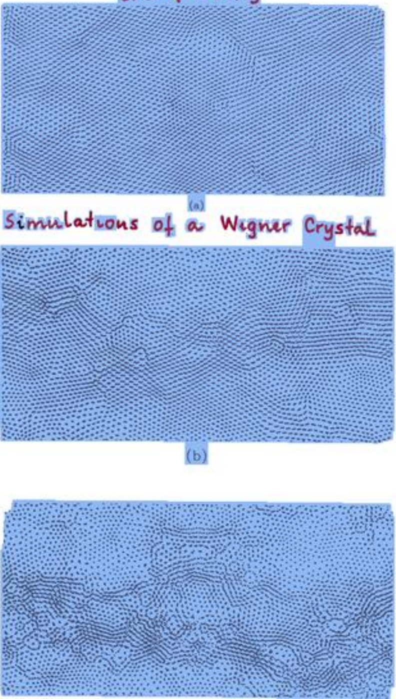

Simulations of a Wigner Crystal

ncreasing disorder ↓

Fingerprint phenomena in plastic flow

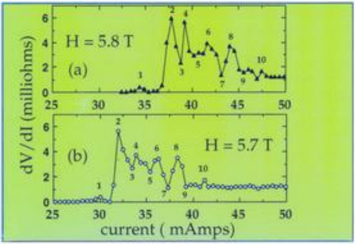

Net voltage : $V = N_{free} \cdot \langle v \rangle$

For elastic flow : N_{free} is independent of v

$dV/dI \sim 1/(d\langle v\rangle/dF) \sim 1/\mu$; μ = friction coeff.

For plastic flow : N_{free} is v-dependent

Peaks are caused by jumps in I-V
i.e., large values of dN_{free}/dI

fingerprint represents a specific sequence of depinning of pieces or "chunks"

Fingerprint of quenched disorder is seen through defects in the F

as the elasticity is tuned by H.

Coexistence of moving and pinned states

First order like depinning transition

Dynamics of a Disordered Flux Line Lattice

S. Bhattacharya and M. J. Higgins
NEC Research Institute, 4 Independence Way, Princeton, New Jersey 08540
(Received 12 October 1992)

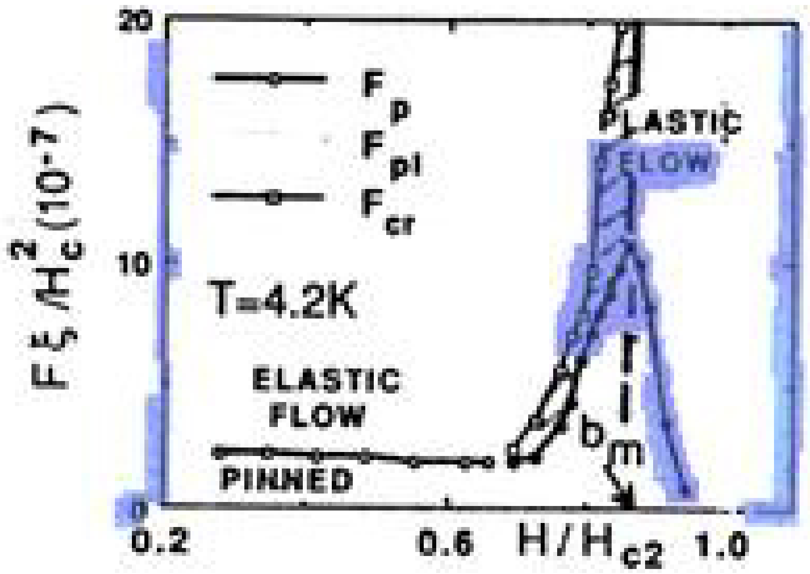

FIG. 3. A nonequilibrium phase diagram of the FLL dynamics. F_p is the conventional depinning threshold separating a pinned FLL from a moving elastic FLL. F_{pl} represents the onset of the plastic flow instability in a defective flux lattice. F_{cr} marks a crossover between the plastic flow and a defect-free elastic flow regime as the defects heal at large drives. b_m marks the Lindemann melting field for a disorder-free FLL. For fields above the peak the pinned FLL may be amorphous. See the text for discussions.

Dynamic Melting of the Vortex Lattice

A. E. Koshelev[1,2,3] and V. M. Vinokur[1]
[1]*Argonne National Laboratory, Argonne, Illinois 60439*
[2]*Kamerlingh Onnes Laboratory, Leiden University, P.O. Box 9506, 2300 RA Leiden, The Netherlands*
[3]*Institute of Solid State Physics, Chernogolovka, Moscow District, 142432, Russia*
(Received 26 April 1994)

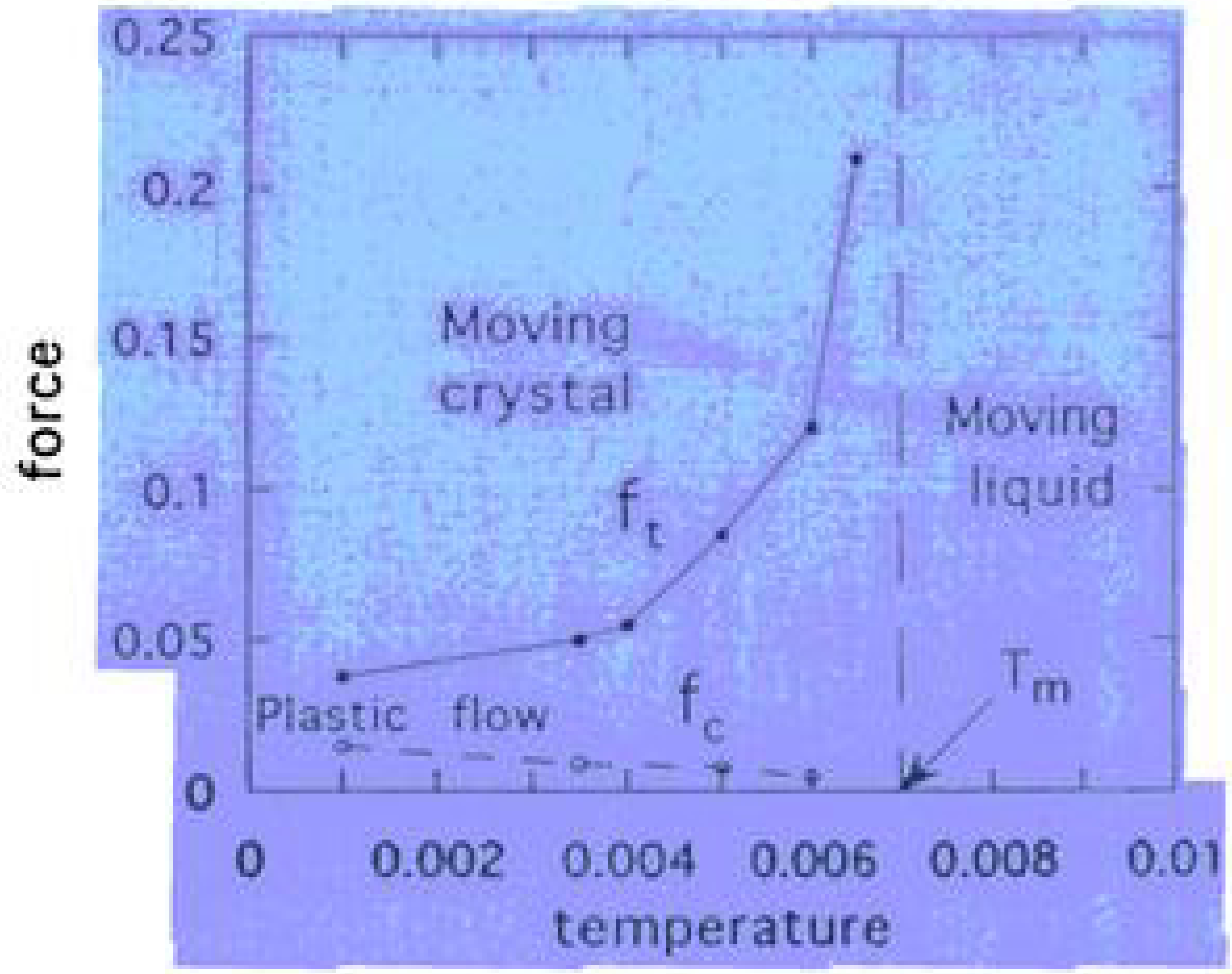

Koshelev and Vinokur :

Current induced crystallization :

Shaking temperature T_{sh} ~ 1/velocity

Vortex matter cools as it moves faster

Orders at large velocity

Also, Larkin, Marchetti & Vinokur PRL ..

Dynamic "Phase Diagram" & "Moving phases"

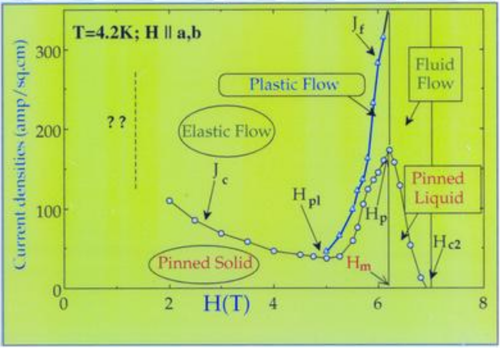

Peak effect = Amorphization of FLL

1. $H < H_{pl}$: Stiff lattice depins coherently :

elastic flow

$H_{pl} < H < H_p$: Soft FLL depins through tears

plastic flow,

"current-induced freezing" at larger forces

"dynamical transition" to elastic flow

3. $H > H_p$: entirely incoherent motion : fluid flow

no transition to coherent motion, force needed for transition diverges around FLL melting

Simulations of Anomalous I-V

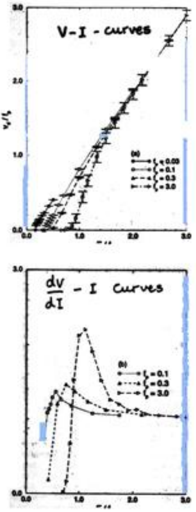

FIG. 3. Drift velocity (a) and differential resistivity dv_d/dF (b) vs driving force for the array with a dense distribution of pinning centers. $N_p/N_v = 133$. The curves obtained by ramping the force up and down are indistinguishable. The error bars represent the value of v_{rms}. Notice that both v_d and F have been divided by f_p to display the data obtained for different values of the pinning force on the same graph.

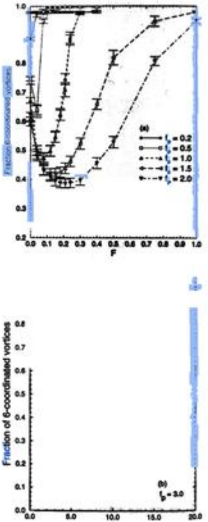

FIG. 4. Fraction of sixfold coordinated vortices vs driving force. (a) is for $N_p/N_v = 0.5$ and the parameter values of Fig. 2. In this case the curves obtained by ramping the force up and down are virtually indistinguishable and no hysteresis is observed. (b) is for $N_p/N_v = 133$, with the parameter values of Fig. 3 and $f_p = 3$. The lower curves are obtained by ramping up the force from an initial disordered configuration of the flux array. Data for both $N_v = 300$ (circles) and $N_v = 1200$ (triangles) are shown to display the finite-size effect. The upper curve (square) is obtained by ramping down

threshold force is large and clearly nonzero for $N_p/N_v = 133$. While we have not determined the threshold value accurately, we find that the numerical estimate agrees

Peak effect and order-disorder transition

P.L. Gammel *et al.*, PRL 80, 833 (1998).

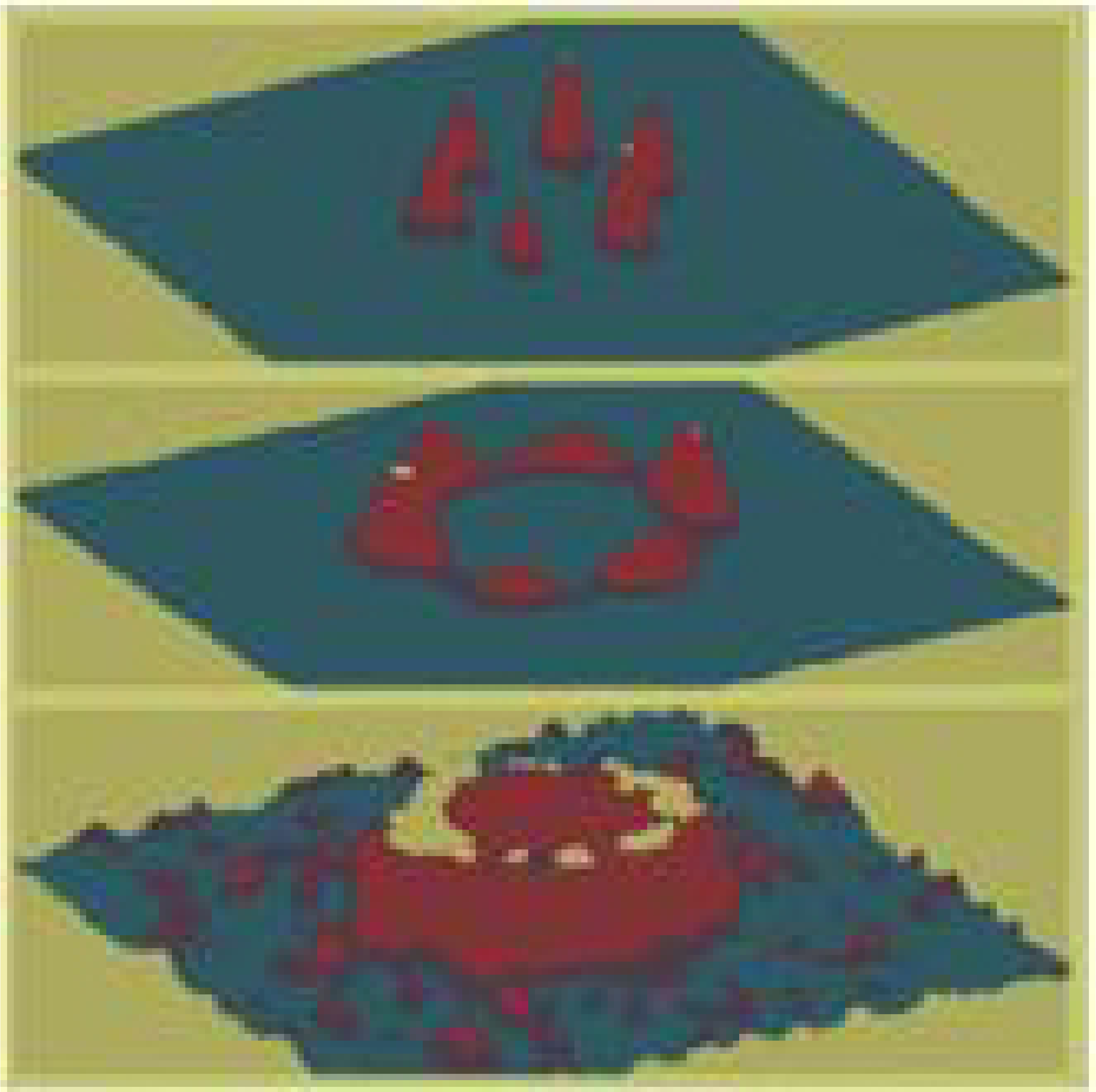

FIG. 2(color). Shown are diffraction patterns from the FLL in three regimes at $T = 4.6$ K. Top: FLL crystal ($H = 1.1$ kOe, $h = 0.47$). Middle: hexatic FLL just below the peak effect ($H = 2.15$, $h = 0.91$). Bottom: ring of scattering from amorphous FLL ($H = 2.25$, $h = 0.96$). The radial width of the peaks determines the positional correlation length ($\sim 1a_0$), the azimuthal width of the peaks gives the orientational correlation length, and rocking through the Bragg gives the longitudinal correlation length ($\sim 100a_0$). Nonuniform peak intensities are instrumental artifacts.

X.S. Ling *et al.* PRL 86, 712 (2001)

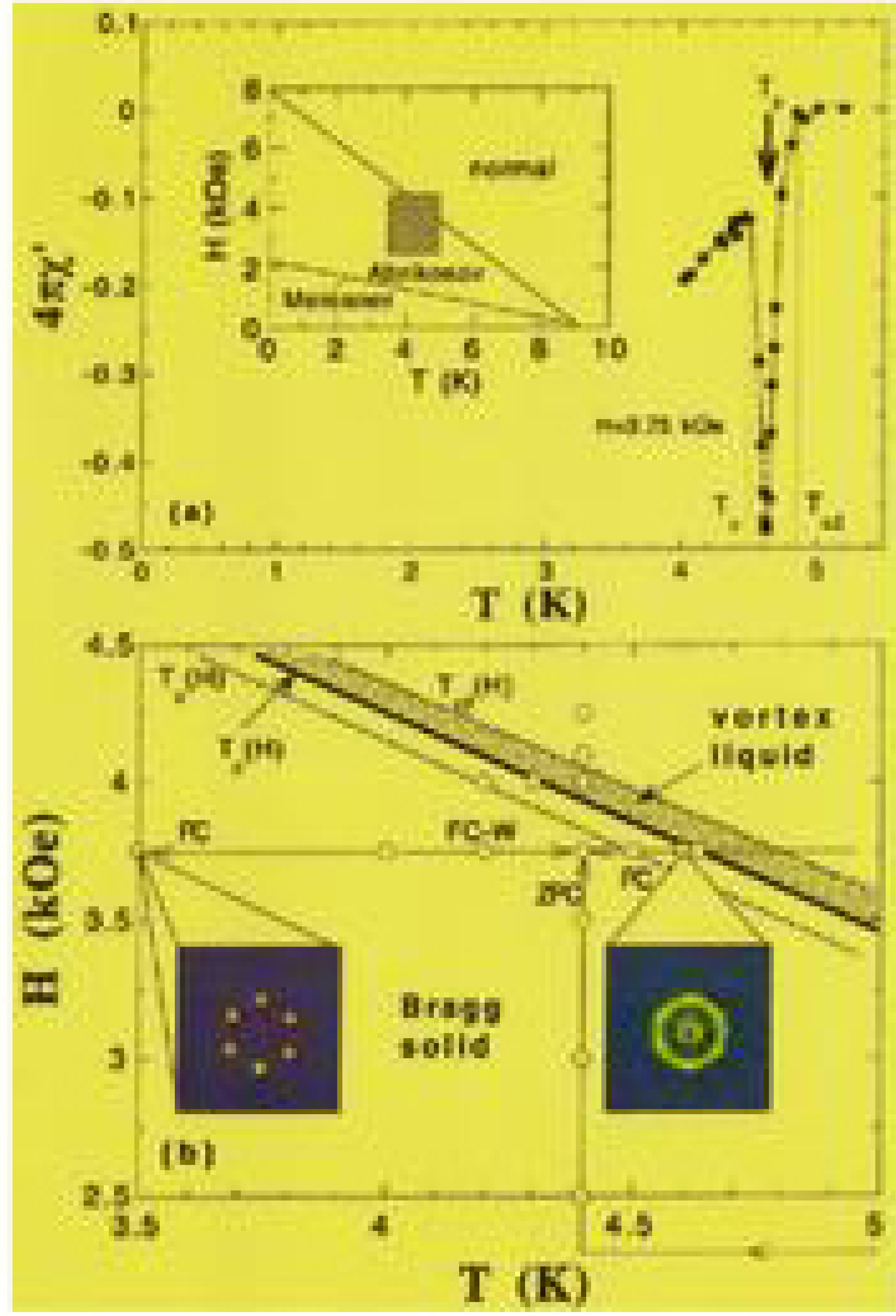

Typical behavior of pinning force at fixed T, varying H

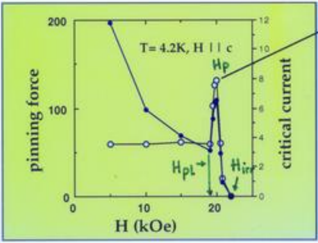

"Peak effect"

H_{pL} : onset of plastic flow

Larkin-Ovchinnikov : Collective Pinning

collective volume : $V_c = R_c^2 . L_c$

Pinning : $W = n_p . \langle f^2 \rangle$; Pinning force density : $F_p = |J_c X B| = (W/V_c)^{1/2}$

$$\boxed{F_p = n_p^2 . f^4 / [16 a^3 . C_{44} . C_{66}^2]}$$

Pinning provides information about correlation of the lattice;

Softer lattice is pinned better

Intermediate H : $C_{66} \sim (H_{c2}-H)^2$; $f \sim (H_{c2}-H)$: $J_c \sim 1/B$; $F_p \sim$ constant

Higher H : Nonlocal C_{44} softens; V_c shrinks rapidly

F_p increases until $R \sim a$ at H_p : amorphous FLL

Even higher H : V constant; $F_p \sim f^2 \sim (H_{c2}-H)$

Peak Effect ~ Amorphization of FLL
but what causes it ?

Power law scaling in two regimes of dynamics

3-D FLL (H ⊥ c)

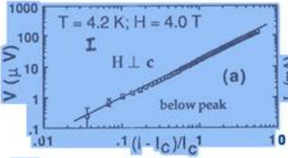

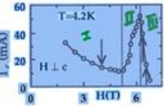

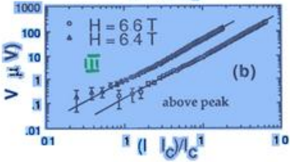

V ~

below peak β 1.3 I

above peak $\beta - 1.7$

Quasi-2D FLL (H || c)

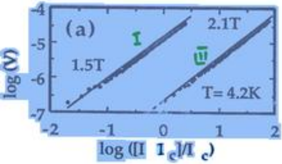

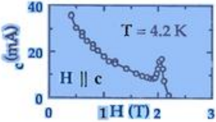

below peak $\beta = 1.15$ I

→ above peak β 1.3 III

Regime Percolative depinning ?

Anomalous frequency dependence in plastic flow

$I = I_{dc} + \delta I \cos \omega t$

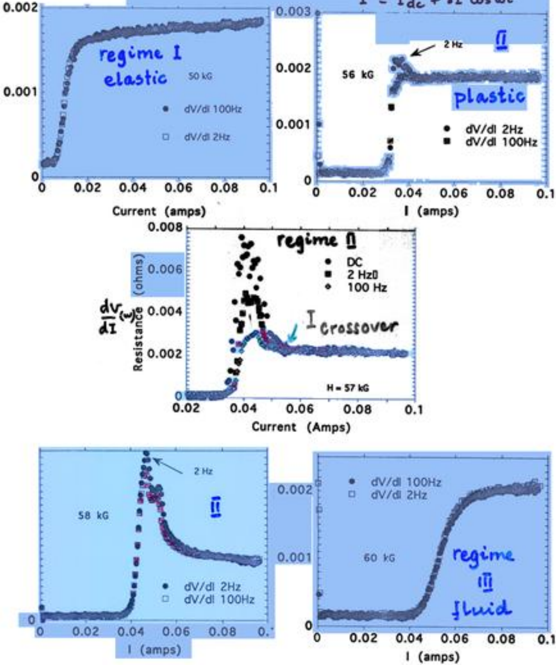

N se in plastic

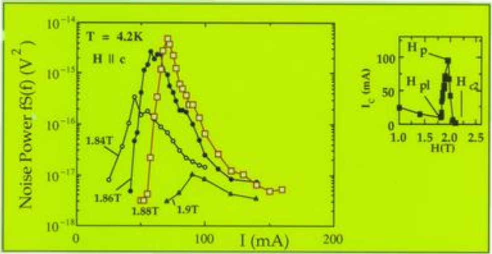

onset of noise coincides with onset of V

noise depletes at large current

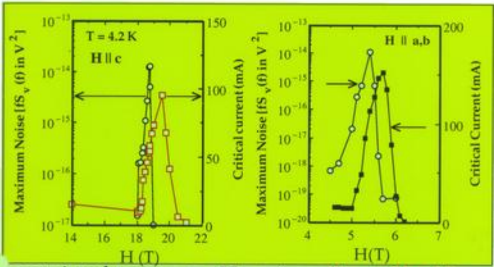

restricted to narrow H-regime : $H_{pl} < H < H_p$

d

1. Rigid Solid : spatially coherent motion
power law F-v curves [critical phenomena?]
L_v ~ system size : non-defective motion
"elastic flow"

2. Soft Solid : incoherent motion at small F
non-power law F-v; first order depinning
Lv ~ large ; a few chunks
"plastic flow"
but, dynamical transition at large F to "elastic flow"

3. Liquid : totally incoherent dynamics
power law F-v; a different case - percolation ?
L_v ~ lattice constant, N chunks
"fluid flow"
but, thermally melted, hence cannot be coherent
even at large forces, quenched disorder is
always relevant (c.f. puddles)

Current status of moving phase studies

Theory : Nature of moving phase and phase transitions

- Moving crystal (Koshelev and Vinokur)
- Moving Bragg glass (Giamarchi and Ledoussal)
- Moving Smectic (Balents, Radzihovsky and Marchetti)
  - Length scales (Balents and MPA Fisher)

Simulations (many):

- confirmation of elastic, plastic and fluid flow
- confirmation of noise in plastic flow
- "chunk" scale and rivers

Experiments on structure of moving phases:

- Bitter decoration:
  - Marchevsky et al, PRL 78, 531 (1997),
  - Pardo et al, PRL 78, 4633 (1997)
- Electron Holography:
  - Tonomura et al , Nature 397, 308 (1999)
- Neutron Diffraction:
  - Yaron et al , Nature 376, 753 (1995)

Expanded to other fields : Colloidal systems, CDW's

Possible analogies with granular systems,...

quite well-ordered with resolution-limited diffraction peaks. An important theoretical advance was made on the basis of numerical simulations by Koshelev and Vinokur[4] who argued that there could be three distinct regimes of flow. For applied currents below the critical current (I_c), these authors found a pinned, moderately disordered solid; at I_c they saw a regime of quite disordered plastic flow; and for currents well above I_c, they found a regime where the moving lattice was quite well ordered, perhaps crystalline. This prediction of a plastic flow regime was confirmed by both SANS[7] and magnetic decoration studies[3,9] of the flowing FLL at I_c.

More recently, Giamarchi and Le Doussal[5] have argued for the existence of a moving-Bragg-glass phase for currents well above I_c. This is a phase free from topological defects, with power-law decay of the positional correlations which are anisotropic with respect to the flow direction. Balents, Marchetti and Radzihovsky[2] have argued instead for a smectic phase. Such a phase is layered in the sense that the vortices flow in channels and are well correlated perpendicular to their flow, but uncorrelated along it. This is consistent with recent numerical simulations[3].

In the magnetic decoration technique used here, the FLL is visualized by evaporating ~50-Å magnetic particles onto the surface of a superconductor held below its transition temperature T_c with a magnetic field applied. The particles follow the field lines of the vortices at the surface of the sample, and land where the vortices are located. Because each pile of magnetic particles has a finite size, the technique is limited to fields below several hundred oersteds. Fortunately, this range of fields covers an interesting region where we can 'tune' the vortex interaction strength relative to the pinning strength, and see a crossover from a smectic structure in the low-field, disorder-dominated limit to a moving Bragg glass in the high-field, interaction-dominated limit.

Our samples were high-quality, single crystals of $NbSe_2$ with typical dimensions of $0.5 \times 0.5 \times 0.2$ mm. They were cleaved just before use to assure a clean surface for the measurement. Samples were cooled down to 4.2 K in a magnetic field applied in the c direction. At low temperatures, the field was removed and the sample was decorated after a certain period of time (t).

Figure 1 shows data from a SQUID (superconducting interference device) measurement of the magnetization of our sample taken as a function of time (t) after the 36 Oe field was removed. The flow velocity (v) at the edge of the sample was extracted from the magnetization using the relation $v = [\partial m(t)/\partial t][A/m(t)P]$ where A is the area, P the perimeter, and $m(t)$ the magnetization. The average lattice constant plotted was obtained using $a_0(t) = [\Phi_0 V/m(t)]^{1/2}$ where V is the sample volume and Φ_0 is the flux quantum. With a one-second decoration time, the plot of the vortex velocity defines two regimes. If the velocity is greater than one vortex lattice constant per second, we find images of vortices in motion. For the regime of vortex velocities less than one lattice constant per second, we obtain quasistatic images of slowly moving vortices. We can work in both regimes. Because of the critical-state profile (independent of velocity regime), we always find a quasistatic, homogeneous structure in the centre of the sample and the critical-state region at the edge. The data shown here is always from the critical-state region.

Our imaging data are shown in Fig. 2. There are three types of images shown for four different regimes (Fig. 2a–d). The first column shows the real-space images (RS) of the FLL, the second the Fourier-transformed (FT) data and the third a Fourier-filtered (FF) real-space image. In the first column, the flow direction is indicated with an arrow. The row of images in Fig. 2a is low-field/low-velocity data, Fig. 2b is low-field/high-velocity, Fig. 2c is high-field/low-velocity and Fig. 2d is high-field/high-velocity data.

Because the data in row Fig. 2a are in the quasistatic regime, the

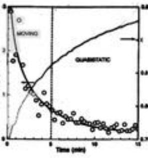

Figure 1 Average vortex velocity and intervortex spacing a_0 as a function of time during flux creep for a sample of $NbSe_2$ at 4.2 K. A field of 36 Oe was originally applied and then removed at $t = 0$. In the moving regime, the vortices move more than the intervortex spacing during an experiment; in the quasistatic regime, the vortices move less than an intervortex spacing during an experiment.

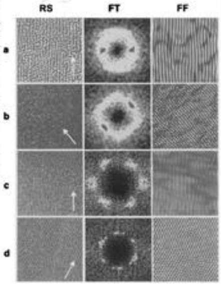

Figure 2 Images of the flux line lattice at different fields and flow velocities. Shown are real space (RS; first column) Fourier-transform space (FT; second column) and Fourier-filtered (FF; third column) images. The real-space images were digitized, flat-fielded on a 20×20 kernel and Lee filtered with a 5×5 kernel. To obtain the Fourier-filtered images, the real and imaginary components of each pixel in the Fourier-transform image were multiplied by a smooth sigmoidal function of their magnitude with a threshold of ~1/3 of the peak magnitude of the FT over the entire image. These data were then inverse-transformed and the absolute value of the inverse transform was used to construct the third column. **a**, Low-field, low-velocity data (5 Oe, 0.2 μm s^{-1}); **b**, low-field, high-velocity data (5 Oe, 2.5 μm s^{-1}); **c**, high-field, low-velocity data (25 Oe, 0.2 μm s^{-1}); **d**, high-field, high-velocity data (25 Oe, 3 μm s^{-1}). Rows **a** and **b** show a smectic vortex lattice; **c** and **d** show a moving-Bragg-glass state. The arrows in the first column show the direction of flow.

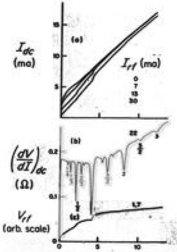

FIG. 1. Data taken at $T = 1.36$ K, $H = 80$ G, and $f = 96$ MHz on a 1000-Å × 1.27-mm × 2.54-mm Al film. (a) dc current for several rf current levels, (b) differential dc resistivity, and (c) rf voltage plotted against dc electric field. Values of the rf current and the ratio n/n' are also shown.

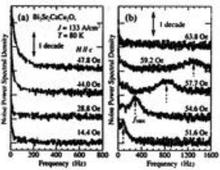

FIG. 2. Conduction noise spectra for selected magnetic fields under 133 A/cm^2 at 80 K. Ticks in the ordinate indicate a noise level of 10^{-18} V^2/Hz for the data at each magnetic field and solid arrows indicate one decade of the noise power spectral density. Typical BBN and NBN structures are shown in (a) and (b), respectively. The dashed arrows indicate the peak position of the NBN.

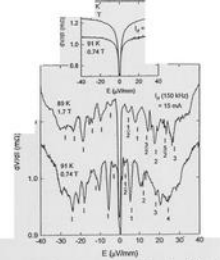

FIG. 1. The differential resistance dV/dI vs the dc electric field E in an untwinned $YBa_2Cu_3O_{6.93}$ crystal at 89 and 91 K in the presence of an rf current I_d (crystal size is $1.5 \times 0.50 \times 0.055$ mm^3). Interference between I_d and the washboard oscillations of the vortex lattice produces steps in the time-averaged velocity $\langle v \rangle$, which appear as negative peaks in dV/dI. The peaks occur when ω and ω_{ext} are harmonically related. Vertical bars, indexed by p/q, indicate the position of the peaks predicted by $E'_{p/q} = (p/q)\omega_{ext} aB/2\pi$, assuming that all vortices between the voltage leads are depinned ($f = 0$). At 91 K, two series of lines with slightly different washboard

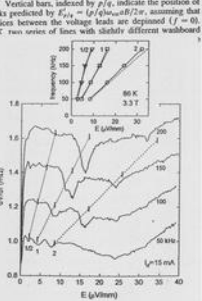

FIG. 2. Four traces of dV/dI vs E taken at 86 K in a 3.3 T field, at different rf frequencies ω_{ext} (the curves are displaced vertically for clarity). As ω_{ext} increases from 50 to 200 kHz, the peak positions shift to higher E fields, in agreement with the washboard effect. Vertical bars indicate the predicted positions $E'_{p/q}$ of the interference peaks with index p/q. The inset compares the observed positions of the peaks (open symbols) with the predicted positions $E'_{p/q}$ assuming the pinned fraction $f = 0$.